Magnetism of $TbPc_2$ on ferromagnetic iron oxide surface

To cite this article: Niccolò Giaconi *et al* 2026 *2D Mater*. **13** 025032

2D Materials

OPEN ACCESS

RECEIVED
23 December 2025

REVISED
7 March 2026

ACCEPTED FOR PUBLICATION
19 April 2026

PUBLISHED
13 May 2026

PAPER

Magnetism of $TbPc_2$ on ferromagnetic iron oxide surface

Niccolò Giaconi[1], Leonardo Tacconi[1], Fabio Santanni[1], Marta Albanesi[1], Guglielmo Albani[2], Isheta Majumdar[2], Luca Schio[3], Matteo Briganti[1], Gianlorenzo Bussetti[2], Edwige Otero[4], Luca Floreano[3], Andrea Caneschi[1,5], Matteo Mannini[1], Giulia Serrano[1,5], Alberto Calloni[2,*] and Lorenzo Poggini[1,6,*]

[1] Department of Chemistry 'Ugo Schiff' DICUS & INSTM Research Unit, University of Florence, Via della Lastruccia 3-13, 50019 Sesto Fiorentino, Italy
[2] Department of Physics, Politecnico di Milano, Piazza Leonardo da Vinci 32, Milan 20133, Italy
[3] Istituto Officina dei Materiali—CNR-IOM Laboratorio TASC, s.s. 14 km 163.5, 34149 Trieste, Italy
[4] Synchrotron-SOLEIL, L'Orme des Merisiers, Saint-Aubin 91192, France
[5] Department of Industrial Engineering—DIEF—and INSTM Research Unit, University of Florence, Via Santa Marta 3, Florence 50139, Italy
[6] Institute for Chemistry of Organo-Metallic Compounds (ICCOM-CNR), Via Madonna del Piano, Sesto Fiorentino, Firenze 50019, Italy
[*] Authors to whom any correspondence should be addressed.

E-mail: alberto.calloni@polimi.it and lorenzo.poggini@cnr.it

Keywords: single molecule magnet, Fe(001), magnetic surfaces, oxide

Supplementary material for this article is available online

Abstract

Thin inorganic films, such as metal oxides, are frequently employed as functional materials for decoupling or optimization of the interaction between molecular magnetic layers and metallic surfaces. In the case of single-molecule magnet (SMM) deposits, an effective decoupling layer can reduce the hybridization with the metallic substrate, which would otherwise suppress their intrinsic magnetic bistability. In this work, we investigate the potential of an ultra-thin Fe oxide layer as a substrate for the Tb(III) bis-phthalocyaninato ($TbPc_2$) SMM in technological platforms. A multi-technique approach was employed to evaluate the integrity of a $TbPc_2$ sub-monolayer (ML) deposit and to determine the molecular adsorption geometry at the surface. Furthermore, large-scale facilities experiments were performed, and x-ray magnetic circular dichroism was used to probe the magnetic properties of the $TbPc_2$ sub-ML. The central finding is that while the magnetic moments and electronic configuration of the molecule are preserved, the characteristic slow magnetic relaxation is suppressed. This highlights the critical role of substrate phonon stiffness and tunnel barrier thickness in stabilizing the SMM behaviour.

1. Introduction

Molecular spintronics is an expanding research field dedicated to the development of advanced devices for sensing, data storage, and quantum applications by integrating the properties of inorganic and organic materials [1]. Over the past decades, single-molecule magnets (SMMs) have garnered significant attention as fundamental components in spintronic micro- and nano-devices [2–5] due to their low-temperature magnetic bistability [6] and distinctive quantum properties [1]. Among the various SMM systems, the Tb(III) bis-phthalocyaninato ($TbPc_2$) neutral complex, consisting of a Tb(III) ion coordinated by two phthalocyaninato ligands (Pc) in a staggered configuration (~45° relative rotation) [7, 8], has been extensively studied for its slow magnetization dynamics at liquid helium temperatures [7–10]. It is well established that the magnetic behaviour of $TbPc_2$ can be modulated via redox processes: the neutral molecule and its oxidized or reduced (ionic) forms exhibit markedly different hysteresis profiles. Depending on the parity of the charge state (even vs odd), the hysteresis loop can be either 'open' or butterfly-shaped, due to changes in the coupling between the Tb 4*f* orbital moment and the π-radical(s) of the phthalocyanine ligands [9, 11, 12].

Its molecular structure facilitates the formation of monolayer (ML) and sub-ML deposits on solid surfaces. In the bulk phase, $TbPc_2$ exhibits strong uniaxial anisotropy with the easy magnetization axis perpendicular to the Pc rings. The large energy separation between the ground-state doublet ($J_z = \pm 6$) and the first excited state creates an effective barrier of several hundred Kelvin that impedes magnetization reversal, thereby enabling magnetic bistability [7–10]. However, when deposited on different substrates, the magnetic properties of $TbPc_2$ can be significantly influenced by interfacial interactions [13–16]. The planar geometry of the double-decker complex often promotes electronic coupling with the surface through the π-electron system of the ligands. In particular, studies have reported a pronounced suppression of magnetic bistability when $TbPc_2$ forms sub-MLs on bare metallic substrates [17–20]. Conversely, the introduction of decoupling layers, such as graphene or thin MgO films, has been demonstrated to mitigate these effects [21, 22]. Wäckerlin *et al* have shown that a single ML of MgO is insufficient to effectively decouple $TbPc_2$ from a metallic substrate, whereas increasing the MgO thickness to five MLs enhances magnetic bistability [21], yielding a strong magnetic remanence instead of the butterfly-shaped hysteresis loop characteristic of the bulk phase. The mechanisms governing these modifications in SMMs behaviour remain only partially understood. It has been proposed that the reduced phonon dispersion of metal oxides may play a crucial role in enhancing the stability of the magnetic state [22]. Furthermore, charge transfer processes at the interface can modify the crystal field splitting around the Tb(III) ion, leading to an alteration in magnetic relaxation dynamics.

In order to further explore these interfacial effects, we investigated the use of an oxygen-reconstructed iron surface, where O atoms occupy the fourfold hollow sites in between the Fe(001) atoms, resulting in a $p(1 \times 1)$O superstructure [23, 24], as an alternative substrate for $TbPc_2$ SMMs. In this scenario, the system has another intriguing possibility of enabling magnetic interactions: the topmost layer, which can be viewed as an ultra-thin oxide layer with a nominal FeO stoichiometry, is grown on ferromagnetic Fe, possibly interacting with $TbPc_2$ molecules, as reported for other ferromagnetic or antiferromagnetic metals [25]. This surface, therefore offers not only the potential to serve as a decoupling layer, but also to mediate a magnetic interaction between the molecules and the underlying layer, this being of particular interest for its potential application in spintronics [26–29].

Oxygen chemisorption profoundly alters the electronic and magnetic properties of Fe(001): spin-polarized scanning tunnel microscopy or scanning tunnel spectroscopy (STM/STS) measurements show the emergence of O-induced resonances at and below the Fermi level, a reversal of the tunnelling spin polarization driven by strong O–Fe hybridization [24]. More recently, spin-resolved momentum microscopy combined with density functional theory with dynamical mean-field theory (DFT + DMFT) has revealed that the same $p(1 \times 1)$O overlayer enhances electron correlation, leading to a pronounced narrowing of the Fe d-bands, a strong reduction of the exchange splitting, and the appearance of many-body satellite features incompatible with a Stoner-like description [30].

In the case of the Fe-$p(1 \times 1)$O surface, FeO hereafter, extensive investigation employing metalated tetraphenyl-porphyrin (MTPP) complexes demonstrated the effectiveness of the oxide layer, in preserving the main electronic and chemical properties of the molecules, with minimal structural modifications [31, 32], while it does not compromise the magnetism of molecules [29, 33].

2. Results and discussion

The structural properties, molecular arrangement and physical–chemical interactions at the interface with the FeO have been investigated by low-energy electron diffraction (LEED) and photoemission spectroscopy techniques, such as x-ray and UV photoelectron spectroscopy (XPS and UPS), and inverse photoemission spectroscopy (IPES) for incremental $TbPc_2$ coverage in the ML range.

The LEED picture of the ultra-thin FeO layer surface is reported in figure 1(a) and is characterized by intense diffraction spots arranged to form a square lattice. Upon molecular deposition (panels b and c), the original pattern from the substrate fades away and a new one emerges. This resembles what has been previously observed on MTPPs layers grown on the same surface [34, 35]. This pattern can be described as the superposition of two square lattices rotated by about $+37°$ with respect to the substrate's $<100>$ directions, as shown in the schematic of panel (c). The square lattice is commensurate with the substrate's one (in real space, $a_{TbPc2} = 5a_{Fe} = 1.43$ nm). These findings are compatible with other literature reports on sub-ML $TbPc_2$ deposition on single crystal substrates [17]. At a nominal coverage of 4 ML, no LEED pattern is visible (figure 1(d)), indicating the loss of long-range molecular ordering in multilayer films as observed in other deposits [36].

STM images of the adsorbed $TbPc_2$ molecules are shown in figure 1(e). The analysis of bare surface before molecular deposition (figure S1) is in line with what is reported in the literature [23]. The molecules displayed their characteristic four-lobed appearance, consistently with previous studies on different substrates, confirming their flat-lying adsorption geometry (Pc planes parallel to the surface)

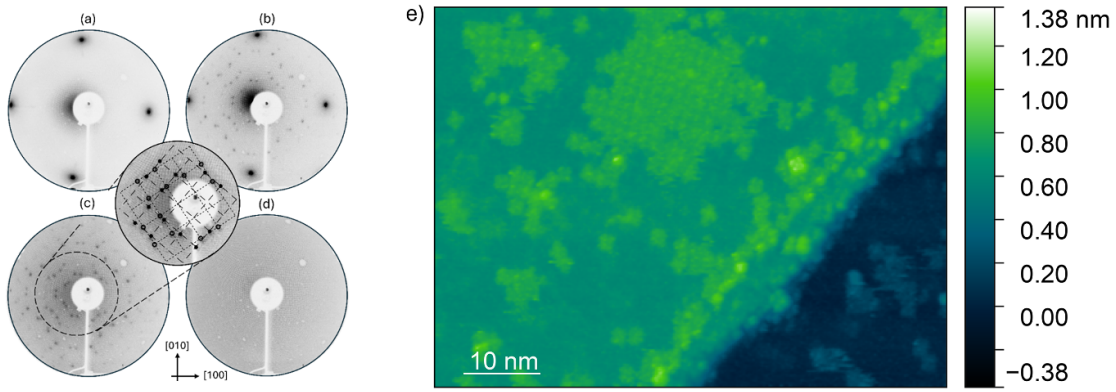

Figure 1. (a) LEED picture of the bare substrate. (b)–(d) LEED pictures of the sample surface for incremental $TbPc_2$ coverage on ultra-thin FeO in monolayers (MLs): 0.5 ML, 1 ML and 4 ML. In the inset, zoom of the central region of the 1 ML pattern with a schematic describing the diffraction pattern as the superposition of two square (5 × 5) lattices tilted with respect to the substrate crystallographic directions. All pictures have been acquired at an electron beam energy of 55 eV and are slightly overexposed to highlight finer details related to diffraction from the molecular layer. (e) STM images of $TbPc_2$ sublimated on ultra-thin FeO (80 pA, 2 V, 65 nm × 50 nm), acquired at 35 K.

with a lateral dimension of the isolated molecules of 1.70 ± 0.15 nm, as observed on both metals and on metal oxides [13, 14, 17, 37, 38]. Interestingly, molecules preferentially assemble into well-ordered square islands rather than remaining dispersed in an irregular arrangement, at variance with what has been obtained on Cu(100) [39], TiO_2 [14], and for CoPc molecules on TiO_2(100) [40]. $TbPc_2$ molecules hence exhibit a low affinity for the substrate, and prefer molecule–molecule packing.

The valence electronic structure has been investigated by UPS and IPES. Results are shown in figure 2. For what concerns filled electronic states (UPS spectra, figure 2(a)), the substrate spectral line shape encompasses the contribution from Fe 3*d* states (# on the red spectrum of figure 2(a)) close to the Fermi energy (E_F), and a sharp peak at a binding energy (BE) of about 4.3 eV (* on the red spectrum of figure 2(a)), representative of photoemission from O 2*p* states [41, 42]. Upon $TbPc_2$ deposition, new features appear, which are related to photoemission from molecules. At nominal ML coverage, the oxygen peak is completely quenched, while a substantial contribution from the Fe substrate is still visible close to E_F, although smeared out by photoelectron scattering through the molecular layer [29, 43]. Overall, the LEED and UPS results (in particular the suppression of the sharp oxygen peak, observed also with MTPPs)[29] convey the idea of a rather uniform covering of the substrate by the molecules, with the completion of the first molecular layer at the nominal coverage of 1 ML.

At multilayer coverage (4 ML), the UPS spectrum mainly reflects the photoemission signal from $TbPc_2$ molecules not directly in contact with the underlying substrate. The line shape is consistent with other literature reports on Pc-based systems (see [44] and references therein). The doublet structure observed close to E_F, featuring two peaks at a BE of about

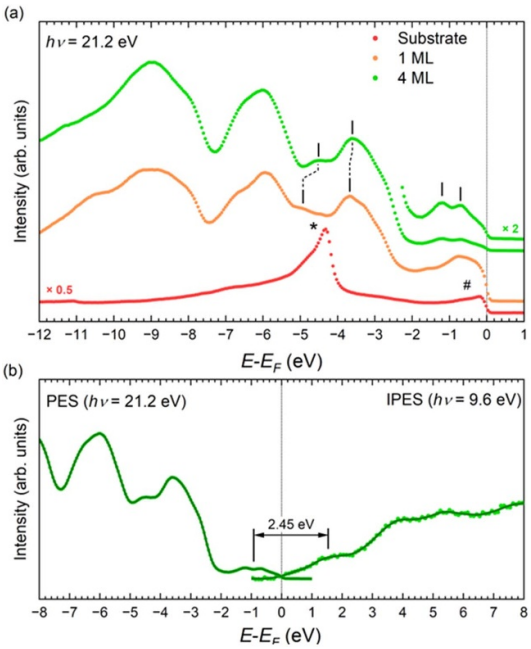

Figure 2. (a) UPS data acquired on the ultra-thin FeO layer and for incremental $TbPc_2$ coverages (1 ML and 4 ML) vertical lines highlight the binding energy position of specific features. Spectra form different samples have been vertically offset for clarity. (b) UPS and IPES characterization of the thick $TbPc_2$ film. Highlighted is the relevant energy gap to be compared with optical absorption experiments.

1.2 eV and 0.7 eV likely arises from the combination of two effects: (i) the π–π interaction between the two phthalocyanine rings, which splits the Pc highest occupied molecular orbital (HOMO) into a completely filled and a half-filled level, given the radical nature of the complex, and (ii) an additional Mott–Hubbard splitting of the latter. The superposition of these two phenomena generates two distinct maxima in the UPS spectrum, in agreement with the model proposed by Fahy *et al* [45–47], suggesting a common

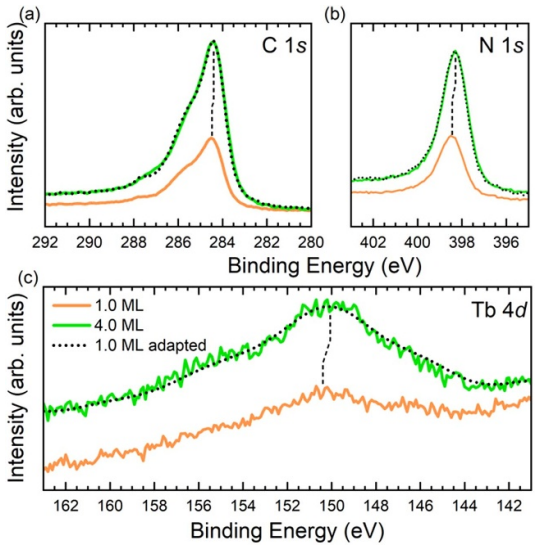

Figure 3. X-ray photoemission spectra acquired on 1 ML and 4 ML $TbPc_2$ films on ultra-thin FeO in the (a) C 1*s*, (b) N 1*s* and (c) Tb 4*d* binding energy regions with Mg Kα ($h\nu = 1253.6$ eV) photons. The 1 ML spectra have been shifted in BE and scaled in intensity (black dotted lines) for better comparison with 4 ML data. In the case of panel (c), this operation was complemented by the application of a smoothing algorithm and the addition of a linear background, in order to account for the high-energy tail related to the contribution of the Fe 3*s* emission peak at lower BEs (not shown). Source satellites have been subtracted from the data. Spectra from different samples have been offset for clarity.

nature of HOMO states in both $LuPc_2$ and $TbPc_2$ molecular species.

Photoemission features from $TbPc_2$ molecules are seen to shift towards smaller BE with increasing coverage, with the magnitude of the shift showing a certain feature-related variability (as highlighted in figure 2(a) with vertical dotted lines). This behaviour is known for many π-conjugated organic systems deposited on metals or oxides and originates from several interfacial effects [48, 49]. At low coverage, the electronic structure is strongly influenced by the molecule–substrate interaction, including charge rearrangement and Pauli push-back, which stabilizes the occupied states and results in higher BEs [50]. As the film becomes thicker, intermolecular interactions progressively dominate and an interface dipole layer forms and stabilizes, leading to a realignment of the molecular levels toward their bulk-like positions [51–54]. In parallel, the coverage-dependent electronic-screening transition from substrate- to molecule-dominated screening contributes to the shift further stand [55]. Because these effects depend on the spatial distribution and character of individual orbitals, the magnitude of the shift is feature-dependent. Overall, such coverage-induced BE shifts are fully consistent with the standard behaviour observed for phthalocyanine and porphyrin films in UPS studies on several substrates [56–58], including oxides or passivated substrates [51, 59–62].

A complete picture encompassing also empty electronic states is provided for the multilayer film by combining UPS and IPES. According to the STS results of [45] and *ab-initio* calculations [63], contributions from both the Tb core and the Pc macrocycle are expected just above E_F, with the former being identified as the lowest unoccupied molecular orbitals (LUMOs). A monotonous increase in the IPES signal is observed in figure 2(b), the energy region immediately above E_F, culminating in a broad structure settling at about 1.5 eV. Two more intense structures follow at an energy of about 4 eV and 5.5 eV. Nearly the same line shape is shown in literature [64] for $LuPc_2$ molecules (featuring a completely filled 4*f* shell), seemingly confirming a strong similarity between the valence electronic structure of the two species also for empty electronic states. Here, the absence of any clear signal from Tb states can be explained considering the low cross section of IPES transitions involving 4*f* electrons at the low photon energy used for the present characterization [65].

By considering the energy gap between the centroid of HOMO features in filled states and the shoulder at about 1.5 eV in empty states, related to the lowest unoccupied electronic states of the macrocycle ($LUMO_{Pc}$), we retrieve a value of 2.45 eV, roughly 0.5 eV larger than the reported optical absorption maximum of $TbPc_2$ molecules, the so-called Q band at 640–690 nm [66], likely due to exciton formation. As previously specified, the electronic structure of neutral $TbPc_2$ molecules should be characterized by a radical π electron in the antibonding HOMO state (settling close to E_F in figure 2(b)), called the singly occupied molecular orbital (SOMO), and, as a consequence, by a singly unoccupied molecular orbital (SUMO) in empty state. This would result in a *conduction gap* as small as 0.5 eV, in agreement with the narrow-gap semiconducting behaviour observed for these molecules [64]. The UPS and IPES spectra in figure 2(b) for the 4 ML film, although not resolving the SUMO feature explicitly, are fully consistent with its assignment and, considering the analysis of Murdey *et al* [64], provide compelling support for the interpretation that the transport gap is defined by the SOMO–SUMO orbital pair.

To shed light on the molecular properties at the interface, we compared the XPS of 1 ML and 4 ML (figure 3). The 1 ML spectrum shows nearly the same line shape of the one acquired on thicker film. Black dotted lines, obtained from the former spectra after some shifting and rescaling as described in the caption of figure 3, help comparing the two datasets. Overall, the BE position (within few hundreds of meV) and spectral line shape for N 1*s* and C 1*s* features are consistent with literature reports [13, 14, 67]. The measured Tb 4*d* region, dominated by multiplet effects, is also compatible with the available literature on oxidized Tb species [68, 69]. Similarly to UPS, a slight shift of the photoemission features

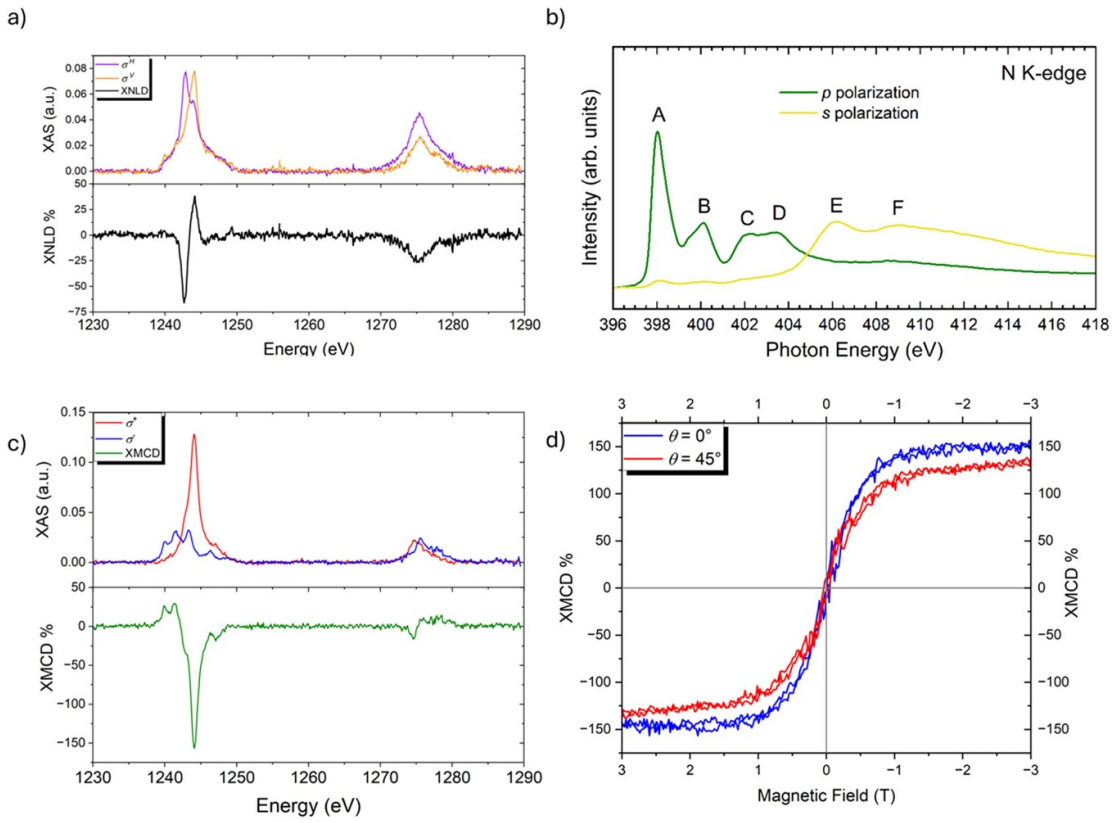

Figure 4. Magnetic and structural characterization of the $TbPc_2$ sub-monolayer on the Fe(001) $p(1 \times 1)$O substrate. (a) XAS with vertical and horizontal light polarization (top) and XNLD (bottom) spectra at the Tb $M_{4,5}$ edge recorded at $\theta = 45°$, $B = 3$ T, and $T = 2.0$ K. (b) XAS acquired at the N K-edge with *p*- and *s*-polarized light. (c) XAS with circular left and right light polarization (top) and XMCD (bottom) spectra at the Tb $M_{4,5}$ edge recorded at $\theta = 0°$, $B = 3$ T, and $T = 2.0$ K. (d) Magnetic hysteresis loop recorded at the Tb M_5 edge at 2.0 K and at $\theta = 0°$ and $\theta = 45°$ with a scan rate of 0.03 T s^{-1}.

towards lower BE in the thicker film is observed also by XPS. A conclusive explanation for this specific phenomenon is not straightforward. The modest change of about 0.1 eV in the sample work function (data not shown) suggests that electrostatic interactions leading to charge transfer from the substrate might not be the only process responsible for the observed behaviour [44, 67], in line with the above discussed UPS spectra. However, especially with reference to XPS results, we emphasize that the above observations exclude the presence of a strong chemical interaction of the first layer of molecules with the substrate, which otherwise would have resulted in broader 1 ML spectra and possibly the presence of additional features at lower-/higher BE [31, 70].

Low-temperature XAS investigations were conducted on the $TbPc_2$ sub-ML deposited on the ultrathin FeO layer to assess its structural and magnetic characteristics of both the molecular and the inorganic layers. The absorption spectra recorded using linear polarized light at the Tb $M_{4,5}$ edge provided key insights. The XNLD spectrum (figure 4(a)) displayed a pronounced negative dichroic signal at 1242.6 eV, confirming the predominant lying-down orientation of the $TbPc_2$ ML, as previously observed via STM.

The orientation of $TbPc_2$ molecules in contact with the substrate has also been evaluated by near edge x-ray absorption fine structure spectroscopy (NEXAFS) performed at the N K-edge. Results are shown in figure 4(b), where the main features are labelled with letters from A to F, according to the literature [71].

Features from A to D represent N $1s \rightarrow \pi^*$ transitions, with peaks A and B related to transitions to the molecular $LUMO_{Pc}$ and $LUMO_{Pc} + 1$ orbitals, while features E and F are related to N $1s \rightarrow \sigma^*$ transition. Tb empty electronic states are not expected to contribute strongly to the measured spectral lineshape, given their different spatial localization with respect to N 1*s* core hole. Features A–D are most prominent in the *p*-polarization spectrum, and they almost vanish in *s*-polarization, thus indicating a preferential orientation of π^* states perpendicular to the substrate, i.e. a flat lying configuration of the Pc subunits. The same conclusion can be drawn from the inspection of the *s*-polarization spectrum, where the features E–F, σ^* being states oriented in the plane of the Pc subunits, display a reversed NEXAFS linear dichroism [72, 73]. A residual contribution from features A–D is also visible in the *s*-polarization spectrum, albeit with a very small intensity, encompassing about 5% of the intensity of the same features in the *p*-polarization spectrum. This very small signal can be either related to molecules at defects, like step

edges, or to a small distortion of the molecular skeleton, which is intrinsic of the tetrapyrroles chelation to the central Tb(III) ion (umbrella-like), rather than to an average tilt angle (of the order of 10°) of $TbPc_2$ molecules with respect to the Fe surface. Overall, the NEXAFS results suggest the formation of a layer of $TbPc_2$ molecules whose Pc subunits are nearly flat with respect to the substrate surface. To further support these experimental findings, we also simulated the XNLD spectrum at Tb $M_{4,5}$ edge using the protocol described in the methods section. The simulated spectrum closely matches the experimental one when assuming the Pc axis to be perpendicular to the surface (figure S2(a)).

The x-ray magnetic circular dichroism (XMCD) measurements at 2.0 K (figure 4(c)) corroborates the characteristic M_5 edge dichroic response of Tb(III) ions at 1244.1 eV, revealing a dichroism of approximately 135%, consistent with prior studies on $TbPc_2$ thin films exhibiting a comparable absorption geometry [13, 14]. The XMCD measurement at the Fe $L_{2,3}$ edge (figures S3(a) and S3(b)) and the relative magnetic field scans (hysteresis loops) (figure S3(c)), obtained by monitoring the trend of the XMCD signal at its maximum with the field, reveal a strong in-plane magnetization anisotropy of the film, as reported in literature [74, 75]. Hysteresis loops were recorded at 2.0 K (see experimental section), and at angles $\theta = 0°$ and 45°, θ being the angle between the propagation vector of the light, equal to the direction of the magnetic field, and the normal to the surface [76]. Field and angular dependence of the XMCD signal at the Fe $L_{2,3}$ edge (figure S3) confirms the strong magnetic in-plane anisotropy, which matches the expected one for this type of sample [75]. By applying the XMCD sum rules [75–77] to the spectra recorded at the Fe $L_{2,3}$ edges (figure S4), the orbital ($m_{orb} = 0.08\ \mu B$) and spin ($m_{spin} = 2.22\ \mu B$) moments were estimated and the resulting ratio $m_{orb}/m_{spin} = 0.034$ is in line with reported data [23, 75, 78].

The spectral profile, confirmed the presence of a fully saturated Tb(III) system with a total angular momentum $J = L + S = 6$ [16, 37]. To further consolidate this evidence, the experiment results reported in (figure S3(b)) were compared with simulated XMCD spectra at different incidence angles (0° and 45°, figures S2(c) and (d)). The remarkable agreement between the relative XMCD intensities provides compelling validation of our interpretation and highlights the robustness of the system's magnetic configuration. A complete picture is reported in table S1.

No significant hysteretic response was observed for the Tb M_5 edge at $\theta = 0°$ and at $\theta = 45°$, contrarily to bulk-phase or when $TbPc_2$ is deposited on other surfaces (figure 4(d)) [14, 15, 21, 22]. This behaviour differs from that reported for MgO films, where strong magnetic remanence was detected. The direct comparison with MgO is, however, complicated by differences in film thicknesses. Indeed, studies on MgO multilayers (up to 6 ML) demonstrated an increase in $TbPc_2$ magnetic remanence, coinciding with reduced electron scattering from the metal substrate to the molecule [79, 80]. Our work provides direct evidence that no significant exchange is occurring between $TbPc_2$ and the Fe(001) through the FeO ML, at variance with what observed on other magnetic substrate [81–84]. We remark that the decoupling effect from the underneath metal substrate has not been detected on different ultrathin oxides, such TiO_2 films [13, 14].

3. Conclusion

XPS, UPS, IPES and STM analyses confirmed the preservation of $TbPc_2$ molecular integrity when a thermal deposition protocol is adopted to grow ML deposits on an ultra-thin FeO layer grown on Fe(001). LEED pattern and STM imaging revealed a strong adsorption affinity of this SMM for this surface, leading to the presence of well-organized surface arrangements of molecules; both characterization, flanked by XNLD and NEXAFS spectra, indicated a preferential lying-down orientation of $TbPc_2$ molecules at variance with some other oxide surfaces [16, 37].

The absence of magnetic hysteresis in $TbPc_2$/FeO/Fe(001), despite the preservation of the Tb (III)ground state, provides crucial insight into the hierarchy of relaxation mechanisms. Unlike MgO films (>2/3 ML), which act as rigid barriers [79, 85], our ∼1 ML FeO layer (i.e. the maximum achievable thickness, under our experimental conditions, appears insufficient to decouple the molecule from the phononic scattering and heat bath of the substrate [86]. Both theoretical and experimental works on MgO/Ag(100) indicate that the spin–phonon coupling strength is crucial for retaining the spin properties, and that a detrimental effect arises from the thickness reduction of the decoupling layer [43, 79, 85–87]. Moreover, electronic interactions such as orbital hybridization and tunnelling through the surface layer may add further de-excitation mechanisms, as we previously reported on other systems characterized by a smaller bandgap or a semi-metallic nature [14, 15]. The reader is referred to table S3 in the ESI for a more detailed account of these different aspects. Our findings confirm that ultra-thin decoupling oxide layers do not effectively prevent $TbPc_2$ SMM system from fast relaxation mechanisms, at variance with stiff MgO layer [21, 22], but hinder strong magnetic exchange coupling with magnetic iron substrates, both preserving, on average, their magnetic moment. Therefore, the $TbPc_2$/FeO system seems to be an interesting hybrid structure for probing and manipulating spin and electron properties on a local molecular scale by STS experiments [88] as well as for being used as an interface in a hybrid molecule–oxide spintronic junction [2]. This work

highlights the critical role of substrate phonon stiffness in stabilizing the SMM behaviour. Although no hysteresis is observed, the study defines the boundary conditions for SMM behaviour at hybrid interfaces. Using FeO, a correlated, magnetically ordered oxide, we show via XMCD that the Tb moment survives on a magnetic surface without exchange coupling. In the ultrathin limit, electronic hybridization with the metallic substrate prevails over magnetic coupling, providing key design constraints for molecular spintronic architectures.

4. Methods

The oxygen-reconstructed Fe(001) surface, namely Fe-$p(1 \times 1)$O, which consists of an ultra-thin oxide layer with a FeO stoichiometry on top of the metallic bulk, was prepared by exposing the atomically clean (001) surface of a thick (hundreds of nm) Fe film grown on crystalline MgO(001) to 30 l (1 l = 10^{-6} Torr s) of pure grade molecular oxygen. The surface was kept at a temperature of 720 K during oxygen exposure and then briefly heated up to 970 K [89]. $TbPc_2$ films were prepared by evaporation in vacuum (10^{-9} mbar range) from a heated crucible, with the substrate kept at room temperature. The nominal ML thickness was calibrated by assuming a $TbPc_2$ surface density of $4.9 \cdot 10^{17}$ molecules m^{-2}, consistent with the regular arrangement of molecules observed in the present and previous studies [14, 17] and resulting in a deposited amount of $9.6 \cdot 10^2$ μg m^{-2}, measured by a quartz microbalance. The crucible temperature was adjusted around 660 K to yield a deposition rate of about 0.1 ML min^{-1}.

STM measurements were performed with an Omicron VT-STM equipped with an electrochemically etched W tip. The experiments were conducted at 35 K by cooling with liquid helium flux, under a base pressure of 10^{-11} mbar, in order to minimize molecular mobility on the surface.

LEED was performed with a commercial apparatus (Physical Electronics Inc.) equipped with a beam shutter. LEED images were taken at an incident beam energy of 55 eV, by exposing the sample to the electron beam for a few seconds.

XPS and UPS data were acquired by using lab-based MgKα ($h\upsilon$ = 1253.6 eV) and HeI ($h\upsilon$ = 21.2 eV) photon sources and detecting electrons at normal surface emission with a SPECS Phoibos 150 MCD electron analyser, calibrated on the Au $4f_{7/2}$ emission (at a BE of 83.95 $\pm$ 0.04 eV) of a polycrystalline Au foil. The pass energy was set at 20 (0.7) eV for XPS (UPS) yielding a combined (source + analyser) full width at half maximum (FWHM) resolution of about 1.0 (0.05) eV. IPES was performed in the isochromatic mode, i.e. by sending variable energy electrons from a GaAs photocathode to the sample at normal incidence and detecting 9.6 eV photons. The overall FWHM resolution of the spectrometer was of the order of 0.7 eV.

XAS, together with XMCD and XNLD, were carried out at the DEIMOS beamline (SOLEIL synchrotron, France) [90]. The experiments were performed using circular, vertical, and horizontal polarizations of the incident radiation, while the surface sensitivity was ensured through the use of the total electron yield detection mode.

In order to extract the dichroic contributions, the XNLD signal was determined as the difference between the absorption spectra acquired with vertical (σ^V) and horizontal (σ^H) polarization. Analogously, the XMCD signal was obtained as the difference between the spectra measured with left- (σ^-) and right- (σ^+) handed circular polarizations. Both dichroic contributions were subsequently normalized with respect to the edge jump of the isotropic spectrum at the L_3 edge, according to the expression: $\sigma_{XNLD/XMCD}(\%) = 100 \cdot (\sigma^{V/-} - \sigma^{H/+})/ej(L_3)$, where $ej(L_3)$ represents the step height of the absorption edge (edge jump).

Magnetic hysteresis curves were obtained by recording the field dependence of the %XMCD at the Tb M_5 edge (measured at 1244.1 eV and here referred to the pre-edge dichroism at 1233 eV) sweeping the magnetic field between -3 T and 3 T with a scan rate of 2 T min^{-1}. Data treatment for XMCD, XNLD, and hysteresis was performed employing pyDichroX software [91].

The ML sample used for these measurements was prepared in advance under controlled conditions, described above and shipped to the DEIMOS beamline using a UHV suitcase.

Polarized XAS spectra at the Tb $M_{4,5}$ edge were simulated using multiplet ligand field theory within the Quanty scripting framework [81]. Free ion parameters, including interelectronic repulsions and spin-orbit couplings, were obtained from Cowan's code, with the Slater–Condon integrals scaled by 0.8 to account for relativistic corrections. Crystal field surrounding the Tb centre was considered to be purely axial and crystal field parameters were adopted from the literature [7]. All simulation parameters are listed in table S2. The experimental geometry was reproduced in the calculations, and thermal effects were incorporated by weighting the transitions according to the Boltzmann population of the initial states.

NEXAFS experiments were performed at the ALOISA [92] beamline (ELETTRA synchrotron, Italy), employing linearly polarized light in partial electron yield mode. The spectra have been measured with the surface oriented either parallel to the electric field (s-polarization) or closely normal to it (p-polarization), by rotation of the sample

around the photon beam axis (coaxial manipulator), while keeping the surface at a constant grazing angle of 6° (constant illuminated area). The photon flux normalization and the energy calibration are described in [54]. The energy resolution was set to 80 meV. The beamline is equipped with all the necessary tools for the *in-situ* preparation of the samples.

Acknowledgments

The authors acknowledge the financial support from the National Recovery and Resilience Plan (NRRP), Mission 4 Component 2 Investment 1.3 -Call for tender No. 341 of 15/03/2022 of Italian Ministry of University and Research funded by the European Union—NextGenerationEU, award number PE0000023, Concession Decree No. 1564 of 11/10/2022 adopted by the Italian Ministry of University and Research, CUP D93C22000940001, Project title 'National Quantum Institute', the Italian Ministry of Education and Research (MUR) through PRIN, CROQUET (CUP: B53D23015490006) and FUTURO (CUP: 53D23009110006) is also acknowledged. Project funded under the National Recovery and Resilience Plan (NRRP), Mission 4 Component 2 Investment 1.3, Call for tender No. 1561 of 11.10.2022 of Ministero dell'Università e della Ricerca (MUR); funded by the European UnionNextGenerationEU, Project code PE0000021, CUP B53C22004060006—'SUPERMOL', 'Network 4 Energy Sustainable Transition, NEST'.

I.M. acknowledges financial support from the Italian Ministry of University and Research (MUR), within the framework of the implementation of the National Recovery and Resilience Plan (PNRR), Mission 4 Component 2 Investment 1.2 and in accordance with the Operational Arrangements signed between the European Commission and the Ministry of Economy and Finance on 22/12/2021, Grant Protocol No. SOE_0000076, CUP D43C22004190001, Project MOXOPIF. We acknowledge the DEIMOS beamline of the SOLEIL Synchrotron for providing beam time under Project No. 20231814. The authors acknowledge the technical support and facilities from the Interdepartmental Research Unit 'MatchLab' of the University of Florence.

Data availability statement

All data that support the findings of this study are included within the article (and any supplementary files).

Authors' contributions

L.P., G.S., AL.C., G.B. conceptualised the work, F.S. carried out the synthesis of the complex; L.T. carried out the XAS simulations; N.G., L.P, G.A., G.S. investigation, data curation; I.M., L.F., L.S., E.O., M.A., M.B., F.S., L.T., investigation; M.M., G.S., G.B. writing—review and editing; L.P., AL.C. writing-original draft; writing-review and editing; resources; G.S., M.M. A.C., resources and mentoring.

Author contributions

Niccolò Giaconi 0000-0003-2118-8308
Data curation (equal), Formal analysis (equal)

Leonardo Tacconi 0009-0003-5145-1047
Formal analysis (equal)

Fabio Santanni 0000-0002-0506-8333
Data curation (equal), Formal analysis (equal)

Marta Albanesi 0009-0007-0017-6136
Investigation (equal)

Isheta Majumdar 0000-0002-7705-9970
Investigation (equal)

Luca Schio 0000-0001-8101-4022
Investigation (equal)

Matteo Briganti 0000-0001-8576-3792
Investigation (equal)

Gianlorenzo Bussetti 0000-0001-8556-8014
Conceptualization (equal), Writing – review & editing (equal)

Edwige Otero 0000-0002-3546-3908
Investigation (equal)

Luca Floreano 0000-0002-3654-3408
Investigation (equal)

Matteo Mannini 0000-0001-7549-2124
Funding acquisition (equal), Writing – review & editing (equal)

Giulia Serrano 0000-0001-7953-7780
Conceptualization (equal), Funding acquisition (equal), Investigation (equal)

Alberto Calloni 0000-0002-7389-2703
Conceptualization (equal), Writing – original draft (equal), Writing – review & editing (equal)

Lorenzo Poggini 0000-0002-1931-5841
Conceptualization (equal), Data curation (equal), Formal analysis (equal), Funding acquisition (equal), Investigation (equal), Writing – original draft (equal), Writing – review & editing (equal)

References

[1] Gatteschi D, Sessoli R and Villain J 2006 *Molecular Nanomagnets* vol 54 (Oxford University Press)

[2] Cucinotta G *et al* 2017 Tuning of a vertical spin valve with a monolayer of single molecule magnets *Adv. Funct. Mater.* **27** 1703600

[3] Bogani L and Wernsdorfer W 2008 Molecular spintronics using single-molecule magnets *Nat. Mater.* **7** 179–86

[4] Urdampilleta M, Nguyen N-V, Cleuziou J-P, Klyatskaya S, Ruben M and Wernsdorfer W 2011 Molecular quantum spintronics: supramolecular spin valves based on single-molecule magnets and carbon nanotubes *Int. J. Mol. Sci.* **12** 6656–67

[5] Ganzhorn M, Klyatskaya S, Ruben M and Wernsdorfer W 2013 Carbon nanotube nanoelectromechanical systems as magnetometers for single-molecule magnets *ACS Nano* **7** 6225–36

[6] Christou G, Gatteschi D, Hendrickson D N and Sessoli R 2000 Single-molecule magnets *MRS Bull.* **25** 66–71

[7] Ishikawa N, Sugita M, Okubo T, Tanaka N, Iino T and Kaizu Y 2003 Determination of ligand-field parameters and f-electronic structures of double-decker bis (phthalocyaninato) lanthanide complexes *Inorg. Chem.* **42** 2440–6

[8] Ishikawa N, Sugita M, Ishikawa T, Koshihara S-Y and Kaizu Y 2003 Lanthanide double-decker complexes functioning as magnets at the single-molecular level *J. Am. Chem. Soc.* **125** 8694–5

[9] Gonidec M, Amabilino D B and Veciana J 2012 Novel double-decker phthalocyaninato terbium (III) single molecule magnets with stabilised redox states *Dalton Trans.* **41** 13632

[10] Malavolti L, Mannini M, Car P E, Campo G, Pineider F and Sessoli R 2013 Erratic magnetic hysteresis of $TbPc_2$ molecular nanomagnets *J. Mater. Chem. C* **1** 2935–42

[11] Blackmore W J A, Chen Y, Klyatskaya S, Mattioni A, Fuhr O, Ruben M and Chilton N F 2025 Re-examination of the relaxation dynamics of $[TbPc_2][NBu_4]$ *Inorg. Chem.* **64** 17745–53

[12] McAdams S G, Ariciu A-M, Kostopoulos A K, Walsh J P S and Tuna F 2017 Molecular single-ion magnets based on lanthanides and actinides: design considerations and new advances in the context of quantum technologies *Coord. Chem. Rev.* **346** 216–39

[13] Serrano G, Sorrentino A L, Poggini L, Cortigiani B, Goletti C, Sessoli R and Mannini M 2021 Substrate mediated interaction of terbium (III) double-deckers with the TiO_2 (110) surface *Phys. Chem. Chem. Phys.* **23** 12060–7

[14] Sorrentino A L *et al* 2021 A $TbPc_2$ sub-monolayer deposit on a titanium dioxide ultrathin film: magnetic, morphological, and chemical insights *J. Mater. Chem. C* **9** 15011–7

[15] Serrano G, Velez-Fort E, Cimatti I, Cortigiani B, Malavolti L, Betto D, Ouerghi A, Brookes N B, Mannini M and Sessoli R 2018 Magnetic bistability of a $TbPc_2$ submonolayer on a graphene/SiC(0001) conductive electrode *Nanoscale* **10** 2715–20

[16] Malavolti L *et al* 2013 Magnetism of $TbPc_2$ SMMs on ferromagnetic electrodes used in organic spintronics *Chem. Commun.* **49** 11506

[17] Serrano G, Wiespointner-Baumgarthuber S, Tebi S, Klyatskaya S, Ruben M, Koch R and Müllegger S 2016 Bilayer of terbium double-decker single-molecule magnets *J. Phys. Chem. C* **120** 13581–6

[18] Katoh K *et al* 2009 Direct observation of lanthanide (III)-phthalocyanine molecules on Au(111) by using scanning tunneling microscopy and scanning tunneling spectroscopy and thin-film field-effect transistor properties of Tb(III)- and Dy(III)-phthalocyanine molecules *J. Am. Chem. Soc.* **131** 9967–76

[19] Komeda T, Isshiki H, Liu J, Zhang Y-F, Lorente N, Katoh K, Breedlove B K and Yamashita M 2011 Observation and electric current control of a local spin in a single-molecule magnet *Nat. Commun.* **2** 217

[20] Ara F, K Q Z, Hou J, Komeda T, Katoh K and Yamashita M 2016 A scanning tunneling microscopy study of the electronic and spin states of bis(phthalocyaninato)terbium(III) ($TbPc_2$) molecules on Ag(111) *Dalton Trans.* **45** 16644–52

[21] Wäckerlin C *et al* 2016 Giant hysteresis of single-molecule magnets adsorbed on a nonmagnetic insulator *Adv. Mater.* **28** 5195–9

[22] Studniarek M *et al* 2019 Understanding the superior stability of single-molecule magnets on an oxide film *Adv Sci.* **6** 1901736

[23] Donati F *et al* 2009 Scanning tunneling spectroscopy of the Fe(001)−p(1×1)O surface *Phys. Rev. B* **79** 195430

[24] Tange A, Gao C L, Yavorsky B Y, Maznichenko I V, Etz C, Ernst A, Hergert W, Mertig I, Wulfhekel W and Kirschner J 2010 Electronic structure and spin polarization of the Fe(001)−p(1×1)O surface *Phys. Rev. B* **81** 195410

[25] Moreno Pineda E, Komeda T, Katoh K, Yamashita M and Ruben M 2016 Surface confinement of $TbPc_2$-SMMs: structural, electronic and magnetic properties *Dalton Trans.* **45** 18417–33

[26] Chylarecka D, Wäckerlin C, Kim T K, Müller K, Nolting F, Kleibert A, Ballav N and Jung T A 2010 Self-assembly and superexchange coupling of magnetic molecules on oxygen-reconstructed ferromagnetic thin film *J. Phys. Chem. Lett.* **1** 1408–13

[27] Avvisati G, Gargiani P, Mariani C and Betti M G 2021 Tuning the magnetic coupling of a molecular spin interface via electron doping *Nano Lett.* **21** 666–72

[28] Cojocariu I, Baranowski D, Feyer V, Jugovac M and Schneider C M 2025 Spin and momentum mapping of highly oriented spinterfaces *Nano Lett.* **25** 17138–44

[29] Jagadeesh M S, Calloni A, Brambilla A, Picone A, Lodesani A, Duò L, Ciccacci F, Finazzi M and Bussetti G 2019 Room temperature magnetism of ordered porphyrin layers on Fe *Appl. Phys. Lett.* **115** 082404

[30] Janas D M *et al* 2023 Enhancing electron correlation at a 3d ferromagnetic surface *Adv. Mater.* **35** 2205698

[31] Bussetti G, Calloni A, Celeri M, Yivlialin R, Finazzi M, Bottegoni F, Duò L and Ciccacci F 2016 Structure and electronic properties of Zn-tetra-phenyl-porphyrin single- and multi-layers films grown on Fe(001)-p(1 × 1)O *Appl. Surf. Sci.* **390** 856–62

[32] Orbelli Biroli A *et al* 2021 Out-of-plane metal coordination for a true solvent-free building with molecular bricks: dodging the surface ligand effect for on-surface vacuum self-assembly *Adv. Funct. Mater.* **31** 2011008

[33] Albani G, Calloni A, Picone A, Brambilla A, Capra M, Lodesani A, Duò L, Finazzi M, Ciccacci F and Bussetti G 2021 An in-depth assessment of the electronic and magnetic properties of a highly ordered hybrid interface: the case of nickel tetra-phenyl-porphyrins on Fe(001)–p(1 × 1)O *Micromachines* **12** 191

[34] Calloni A *et al* 2020 Cobalt atoms drive the anchoring of Co-TPP molecules to the oxygen-passivated Fe(0 0 1) surface *Appl. Surf. Sci.* **505** 144213

[35] Fratesi G, Achilli S, Ugolotti A, Lodesani A, Picone A, Brambilla A, Floreano L, Calloni A and Bussetti G 2020 Nontrivial central-atom dependence in the adsorption of M-TPP molecules (M = Co, Ni, Zn) on Fe(001)- p(1×1)O *Appl. Surf. Sci.* **530** 147085

[36] Perfetti M, Serri M, Poggini L, Mannini M, Rovai D, Sainctavit P, Heutz S and Sessoli R 2016 Molecular order in buried layers of $TbPc_2$ single-molecule magnets detected by torque magnetometry *Adv. Mater.* **28** 6946–51

[37] Margheriti L *et al* 2010 X-ray detected magnetic hysteresis of thermally evaporated terbium double-decker oriented films *Adv. Mater.* **22** 5488–93

[38] Serrano G *et al* 2022 Magnetic molecules as local sensors of topological hysteresis of superconductors *Nat. Commun.* **13** 3838

[39] Deng Z, Rauschenbach S, Stepanow S, Klyatskaya S, Ruben M and Kern K 2015 Self-assembly of

bis(phthalocyaninato)terbium on metal surfaces *Phys. Scr.* **90** 098003
[40] Ishida N and Fujita D 2012 Adsorption of Co-phthalocyanine on the rutile TiO_2 (110) surface: a scanning tunneling microscopy/spectroscopy study *J. Phys. Chem. C* **116** 20300–5
[41] Fink R L, Mulhollan G A, Andrews A B, Erskine J L and Walters G K 1992 Spin- and angle-resolved photoemission study of chemisorbed p (1×1) O on epitaxial ultrathin Fe/W(001) films *Phys. Rev. B* **45** 9824–33
[42] Calloni A, Fratesi G, Achilli S, Berti G, Bussetti G, Picone A, Brambilla A, Folegati P, Ciccacci F and Duò L 2017 Combined spectroscopic and ab initio investigation of monolayer-range Cr oxides on Fe(001): the effect of ordered vacancy superstructure *Phys. Rev. B* **96** 085427
[43] Giovanelli L *et al* 2013 Interpretation of valence band photoemission spectra at organic-metal interfaces *Phys. Rev. B* **87** 035413
[44] Bufler J, Abraham M, Bouvet M, Simon J and Göpel W 1991 Growth and electronic properties of ultrathin lutetium–diphthalocyanine films studied by electron spectroscopy *J. Chem. Phys.* **95** 8459–66
[45] Vitali L, Fabris S, Conte A M, Brink S, Ruben M, Baroni S and Kern K 2008 Electronic structure of surface-supported bis(phthalocyaninato) terbium(III) single molecular magnets *Nano Lett.* **8** 3364–8
[46] Vrubel I I, Pervishko A A, Herper H, Brena B, Eriksson O and Yudin D 2020 An ab initio perspective on scanning tunneling microscopy measurements of the tunable Kondo resonance of the $TbPc_2$ molecule on a gold substrate *Phys. Rev. B* **101** 125106
[47] Fahy M R, Fujimoto H, Dann A J, Hoshi H, Inokuchi H, Maruyama Y and Willis M R 1990 Electronic structure of $LuPc_2$ and (PcAlF) n oriented thin films using angle resolved photoelectron spectroscopy *Phys. Scr.* **41** 550–4
[48] Koch N 2007 Organic electronic devices and their functional interfaces *Chem. Phys. Chem.* **8** 1438–55
[49] Duhm S, Salzmann I, Bröker B, Glowatzki H, Johnson R L and Koch N 2009 Interdiffusion of molecular acceptors through organic layers to metal substrates mimics doping-related energy level shifts *Appl. Phys. Lett.* **95** 093305
[50] Kera S, Yabuuchi Y, Yamane H, Setoyama H, Okudaira K K, Kahn A and Ueno N 2004 Impact of an interface dipole layer on molecular level alignment at an organic-conductor interface studied by ultraviolet photoemission spectroscopy *Phys. Rev. B* **70** 1–6
[51] Peisert H, Petershans A and Chassé T 2008 Charge transfer and polarization screening at organic/metal interfaces: distinguishing between the first layer and thin films *J. Phys. Chem. C* **112** 5703–6
[52] Greiner M T, Helander M G, Tang W M, Wang Z B, Qiu J and Lu Z H 2012 Universal energy-level alignment of molecules on metal oxides *Nat. Mater.* **11** 76–81
[53] Tsiper E V, Soos Z G, Gao W and Kahn A 2002 Electronic polarization at surfaces and thin films of organic molecular crystals: PTCDA *Chem. Phys. Lett.* **360** 47–52
[54] Floreano L, Cossaro A, Gotter R, Verdini A, Bavdek G, Evangelista F, Ruocco A, Morgante A and Cvetko D 2008 Periodic arrays of Cu-phthalocyanine chains on Au(110) *J. Phys. Chem. C* **112** 10794–802
[55] Ben Hamada B, Souissi A, Menzli S, Arbi I, Akremi A, Chefi C and Derivaz M 2014 Photoemission study of copper phthalocyanine growth on hydrogen-terminated surface: Si(100)2 × 1-H *Thin Solid Films* **567** 96–100
[56] Haidu F, Salvan G, Zahn D R T, Smykalla L, Hietschold M and Knupfer M 2014 Transport band gap opening at metal–organic interfaces *J. Vac. Sci. Technol. A* **32** 040602
[57] Evangelista F, Ruocco A, Corradini V, Donzello M P, Mariani C and Betti M G 2003 CuPc molecules adsorbed on Au(110)-(1×2): growth morphology and evolution of valence band states *Surf. Sci.* **531** 123–30
[58] Poggini L *et al* 2024 Electronic and magnetic properties of a monolayer of VOTPP molecules sublimated on Ag(100) *Adv. Phys. Res.* **3** 2300121
[59] Fukagawa H, Yamane H, Kera S, Okudaira K K and Ueno N 2006 Experimental estimation of the electric dipole moment and polarizability of titanyl phthalocyanine using ultraviolet photoelectron spectroscopy *Phys. Rev. B* **73** 2–5
[60] Grządziel L, Krzywiecki M, Peisert H, Chassé T and Szuber J 2012 Photoemission study of the Si(1 1 1)-native SiO_2/copper phthalocyanine (CuPc) ultra-thin film interface *Org. Electron.* **13** 1873–80
[61] Albani G, Capra M, Lodesani A, Calloni A, Bussetti G, Finazzi M, Ciccacci F, Brambilla A, Duò L and Picone A 2022 Self-assembly of C60 on a ZnTPP/Fe(001)–p(1×1)O substrate: observation of a quasi-freestanding C60 monolayer *Beilstein. J. Nanotechnol.* **13** 857–64
[62] Palmgren P, Claesson T, Önsten A, Agnarsson B, Månsson M, Tjernberg O and Göthelid M 2007 Band bending and structure dependent HOMO energy at the ZnO(0001)-titanyl phthalocyanine interface *Surf. Sci.* **601** 4222–6
[63] Martínez-Flores C, Bolívar-Pineda L M and Basiuk V A 2022 Lanthanide bisphthalocyanine single-molecule magnets: a DFT survey of their geometries and electronic properties from lanthanum to lutetium *Mater. Chem. Phys.* **287** 126271
[64] Murdey R, Bouvet M, Sumimoto M, Sakaki S and Sato N 2009 Direct observation of the energy gap in lutetium bisphthalocyanine thin films *Synth. Met.* **159** 1677–81
[65] Fauster T and Himpsel F J 1984 Energy dependence of cross sections in inverse photoemission *Phys. Rev. B* **30** 1874–6
[66] Colombelli A, Serri M, Mannini M, Rella R and Manera M G 2017 Volatile organic compounds sensing properties of $TbPc_2$ thin films: towards a plasmon-enhanced opto-chemical sensor *Sens. Actuators B* **253** 266–74
[67] Bidermane I, Lüder J, Ahmadi S, Grazioli C, Bouvet M, Brena B, Mårtensson N, Puglia C and Witkowski N 2016 When the grafting of double decker phthalocyanines on Si(100)-2 × 1 partly affects the molecular electronic structure *J. Phys. Chem. C* **120** 14270–6
[68] Ogasawara H, Kotani A and Thole B T 1994 Lifetime effect on the multiplet structure of 4 d x-ray-photoemission spectra in heavy rare-earth elements *Phys. Rev. B* **50** 12332–41
[69] Pan T-M, Chen F-H and Jung J-S 2010 Structural and electrical characteristics of high-k Tb_2O_3 and Tb_2TiO_5 charge trapping layers for nonvolatile memory applications *J. Appl. Phys.* **108** 074501
[70] Cirera B *et al* 2017 Preservation of electronic properties of double-decker complexes on metallic supports *Phys. Chem. Chem. Phys.* **19** 8282–7
[71] Bidermane I *et al* 2013 Experimental and theoretical study of electronic structure of lutetium bi-phthalocyanine *J. Chem. Phys.* **138** 234701
[72] Stöhr J and Outka D A 1987 Determination of molecular orientations on surfaces from the angular dependence of near-edge x-ray-absorption fine-structure spectra *Phys. Rev. B* **36** 7891–905
[73] Willey T M, Bagge-Hansen M, Lee J R I, Call R, Landt L, van Buuren T, Colesniuc C, Monton C, Valmianski I and Schuller I K 2013 Electronic structure differences between H_2-, Fe-, Co-, and Cu-phthalocyanine highly oriented thin films observed using NEXAFS spectroscopy *J. Chem. Phys.* **139** 034701
[74] Dos Santos G, Romá F, Tranchida J, Castedo S, Cugliandolo L F and Bringa E M 2023 Feasibility analysis towards the simulation of hysteresis with spin-lattice dynamics *Phys. Rev. B* **108** 134417
[75] Chen C T, Idzerda Y U, Lin H-J, Smith N V, Meigs G, Chaban E, H H G, Pellegrin E and Sette F 1995 Experimental confirmation of the x-ray magnetic circular dichroism sum rules for iron and cobalt *Phys. Rev. Lett.* **75** 152–5
[76] Duda L-C, Stöhr J, Mancini D C, Nilsson A, Wassdahl N, Nordgren J and Samant M G 1994 Magnetic dichroism in

$L_{2,3}$ emission of Fe, Co, and Ni following energy-dependent excitation with circularly polarized x-rays *Phys. Rev. B* **50** 16758–61
[77] de Groot F M F 1994 X-ray absorption and dischroism of transition metals and their componuds *J. Electron Spectrosc. Relat. Phenom.* **67** 529–622
[78] Chubb S R and Pickett W E 1987 First-principles determination of giant adsorption-induced surface relaxation in p(11) O/Fe(001) *Phys. Rev. Lett.* **58** 1248–51
[79] Garai-Marin H, Ibañez-Azpiroz J, Garcia-Goiricelaya P, Gurtubay I G and Eiguren A 2021 Electron-phonon coupling of Fe-adatom electron states on MgO/Ag(100) *Phys. Rev. B* **104** 195422
[80] Pal J, Smerieri M, Celasco E, Savio L, Vattuone L and Rocca M 2013 Morphology of monolayer MgO films on Ag(100): switching from corrugated islands to extended flat terraces *Phys. Rev. Lett.* **112** 1–5
[81] Haverkort M W 2016 Quanty for core level spectroscopy—excitons, resonances and band excitations in time and frequency domain *J. Phys.: Conf. Ser.* **712** 012001
[82] Lodi Rizzini A *et al* 2011 Coupling single molecule magnets to ferromagnetic substrates *Phys. Rev. Lett.* **107** 177205
[83] Lodi Rizzini A *et al* 2012 Exchange biasing single molecule magnets: coupling of $TbPc_2$ to antiferromagnetic layers *Nano Lett.* **12** 5703–7
[84] Klar D *et al* 2013 Antiferromagnetic coupling of $TbPc_2$ molecules to ultrathin Ni and Co films *Beilstein J. Nanotechnol.* **4** 320–4
[85] Donati F *et al* 2016 Magnetic remanence in single atoms *Science* **352** 318–21
[86] Ossowski T and Kiejna A 2023 Structure and energetics of FeO/Fe(001) interfaces *J. Phys.: Condens. Matter* **35** 465001
[87] Stepanow S *et al* 2010 Spin and orbital magnetic moment anisotropies of monodispersed bis(phthalocyaninato)terbium on a copper surface *J. Am. Chem. Soc.* **132** 11900–1
[88] Reale S, Hwang J, Oh J, Brune H, Heinrich A J, Donati F and Bae Y 2024 Electrically driven spin resonance of 4f electrons in a single atom on a surface *Nat. Commun.* **15** 5289
[89] Albani G, Calloni A, Jagadeesh M S, Finazzi M, Duò L, Ciccacci F and Bussetti G 2020 Interaction of ultra-thin CoTPP films on Fe(001) with oxygen: interplay between chemistry, order, and magnetism *J. Appl. Phys.* **128** 035501
[90] Kappler J-P *et al* 2018 Ultralow-temperature device dedicated to soft x-ray magnetic circular dichroism experiments *J. Synchrotron Radiat.* **25** 1727–35
[91] Cucinotta G n.d. pyDichroX (available at: https://github.com/BeppeC/pyDichroX)
[92] Floreano L *et al* 1999 Performance of the grating-crystal monochromator of the ALOISA beamline at the Elettra Synchrotron *Rev. Sci. Instrum.* **70** 3855–64